

Chapter 16

Mid-Infrared GaInSb/AlGaInSb Quantum Well Laser Diodes Grown on GaAs

G. R. Nash

Abstract The aluminium-gallium-indium-antimonide ($\text{Al}_x\text{Ga}_y\text{In}_{1-x-y}\text{Sb}$) material system offers great promise for efficient laser diode operation across the $3\text{--}5\,\mu\text{m}$ wavelength range. It offers an excellent compromise between the requirements for good electronic and optical confinement and those for low series resistance. In addition, the use of an active region comprising compressively strained Type-I quantum wells (QWs) is predicted to lead to increased gain, which leads to lower threshold current densities and hence reduced non-radiative Auger recombination. In this paper a review of recent progress in the development of this material system is given, including the demonstration of multi-quantum well samples exhibiting photoluminescence up to room temperature, and laser diodes operating up to 219 K.

16.1 Introduction

Efficient, room temperature, mid-infrared semiconductor lasers are required for applications such as gas sensing, free space optical communication, healthcare and missile countermeasures. However, although there has been considerable progress over the last few years, high power room temperature operation in the $3\text{--}4\,\mu\text{m}$ wavelength region still remains challenging. Several competing technologies are therefore being developed, including quantum cascade and interband cascade lasers that utilise sophisticated semiconductor band engineering. In 2007, strain-balanced In-GaAsInAlAs quantum cascade lasers (QCLs) were demonstrated operating at room temperature (RT), with continuous wave (CW) emission at a wavelength of $3.84\,\mu\text{m}$, and with over 100 mW of optical power [1]. However, shifting to shorter wavelengths using this material system is difficult as it is hard to maintain a sufficient conduction- band offset. Lasers fabricated from InAs-AlSb [2] and InGaAs-AlAs(Sb) [3, 4] operate pulsed above room temperature, but CW RT

G. R. Nash

QinetiQ, Malvern Technology Centre, Malvern WR14 3PS, U.K., e-mail: grnash@QinetiQ.com

lasing has not yet been demonstrated. Interband cascade lasers (ICLs) based on Type II InAsGaInSb heterostructures have been demonstrated emitting 59 mW of CW power at 298 K and at a wavelength of 3.74 μm [5].

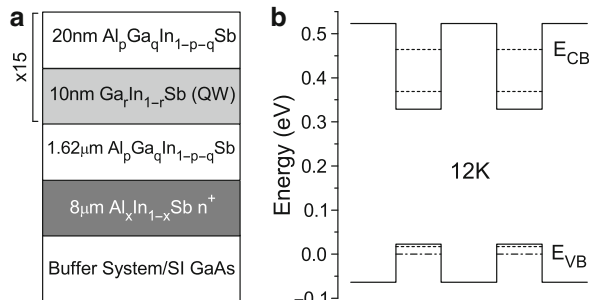


Fig. 16.1 Schematic cross-section (a) showing the generic structure of the PL samples and (b) the calculated energy band diagram of Sample PA under zero net bias and at 12 K. The dashed lines correspond to the two lowest energy electron and hole subbands

An alternative, and somewhat less complicated, approach is to use compressively strained Type I quantum wells and RT lasers emitting at 3.34 μm have recently been demonstrated emitting 50 mW of CW power [6]. We have also previously reported lasing in pulsed mode from Type I multi-quantum well (MQW) lasers, grown on GaAs substrates, based on the GaInSb/AlGaInSb/AlInSb material system [7]. This material system has the potential advantages of being able to achieve band offsets suitable for electronic confinement and also provide sufficiently high compressive strain for lower threshold laser operation [8]. In this paper, recent progress in the development of this material system is reviewed with particular emphasis on the effect of strain on the photoluminescence properties of multi-quantum well samples [9] and the characteristics of laser diodes [10].

16.2 Experimental Method

Samples were grown by molecular beam epitaxy, onto semi-insulating GaAs substrates, at QinetiQ Malvern. Samples for photoluminescence studies consisted of 15 $\text{Ga}_r \text{In}_{1-r} \text{Sb}$ quantum wells (nominal thickness 10 nm) with $\text{Al}_p \text{Ga}_q \text{In}_{1-p-q} \text{Sb}$ barriers (nominal thickness 20 nm), as shown schematically in Fig. 16.1(a), with the corresponding band structure for sample PA shown in Fig. 16.1(b). For each strain iteration two additional structures were grown at the same time: a structure consisting of the bottom $\text{Al}_x \text{In}_{1-x} \text{Sb}$ cladding and $\text{Al}_p \text{Ga}_q \text{In}_{1-p-q} \text{Sb}$ barrier only, and a complete laser structure containing two quantum wells. The composition of the different layers in the MQW samples were determined by performing high resolution x-ray diffraction (XRD) measurements on all the structures grown at each strain iteration,

and by determining the quantum well thickness using transmission electron microscopy. The percentage strain in the quantum wells is defined as $((a_p - a_0)/a_0) \times 100$, where a_0 is the cubic (unstrained) lattice constant, and a_p is the parallel (in-plane) lattice constant. a_0 was obtained from simulation of the (400) rocking curve for the 15 period barrier/QW structure, and a_p from XRD measurement of the barrier lattice parameters i.e. a fully strained system was assumed with a_p (barrier) equal to a_p (QW). This assumption is consistent with the sharpness of the peaks observed in the rocking curve. The composition of each PL sample is summarised in Table 16.1.

The four laser structures (LA, LB, LC and LD) had 0.55%, 0.62%, 0.78% and 1.1% strain in the quantum wells and the generic structure of the diodes is shown schematically in Fig. 16.2(a). Figure 16.2(b) shows the calculated energy band diagram of Structure LA under zero net bias and at 200 K. The diode structure consists of a high Al content $\text{Al}_z\text{In}_{1-z}\text{Sb}$ interfacial layer grown directly onto the GaAs, $\text{Al}_x\text{In}_{1-x}\text{Sb}$ cladding regions, $\text{Al}_p\text{Ga}_q\text{In}_{1-p-q}\text{Sb}$ barriers and two $\text{Ga}_r\text{In}_{1-r}\text{Sb}$ QW active regions.

Table 16.1 Photoluminescence samples

| Sample | $\text{Al}_x\text{In}_{1-x}\text{Sb}$ Cladding | $\text{Al}_p\text{Ga}_q\text{In}_{1-p-q}\text{Sb}$ Barriers | $\text{Ga}_r\text{In}_{1-r}\text{Sb}$ QWs | QW Strain % | PL_{peak} (meV) 12 K | E1-H1 (meV) 12 K | E1-CB (meV) 12 K | H1-VB (meV) 12 K |
|--------|---|--|--|-------------------|-------------------------------------|------------------------|------------------------|------------------------|
| PA | $x = 0.30$ | $p = 0.13, q = 0.17$ | $r = 0.19$ | 0.64 | 364 | 352 | 154 | 81 |
| PB | $x = 0.28$ | $p = 0.14, q = 0.15$ | $r = 0.18$ | 0.71 | 373 | 378 | 152 | 88 |
| PC | $x = 0.37$ | $p = 0.19, q = 0.18$ | $r = 0.22$ | 0.86 | 383 | 383 | 237 | 121 |
| PD | $x = 0.43$ | $p = 0.21, q = 0.20$ | $r = 0.25$ | 0.94 | 396 | 403 | 260 | 130 |

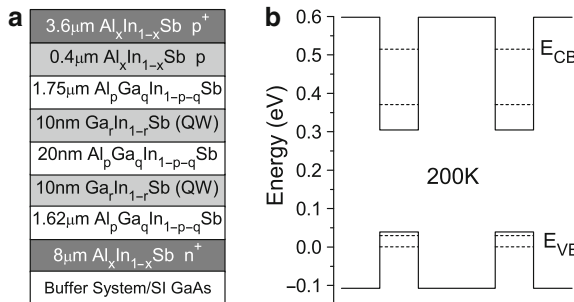


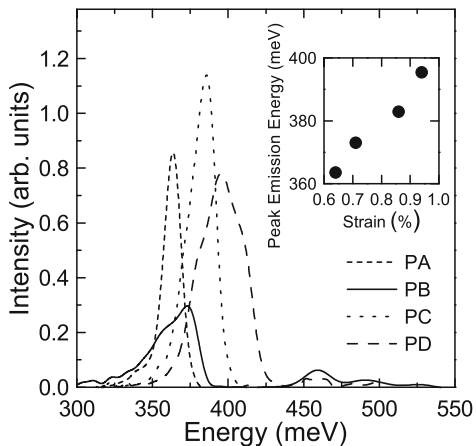
Fig. 16.2 Schematic cross-section (a) showing the generic structure of the laser samples and (b) the calculated energy band diagram of structure LD (under zero net bias) at 200 K. The dashed lines correspond to the two lowest energy electron and hole subbands

The $\text{Al}_z\text{In}_{1-z}\text{Sb}$ layer and bottom $\text{Al}_x\text{In}_{1-x}\text{Sb}$ cladding region together accommodate the lattice mismatch between the GaAs substrate and the GaInSb quantum wells. The composition of each laser sample is summarised in Table 16.2.

Table 16.2 Laser structures

| Sample | $\text{Al}_x\text{In}_{1-x}\text{Sb}$ | $\text{Al}_p\text{Ga}_q\text{In}_{1-p-q}\text{Sb}$ | QWs | QW Strain % | EL_{peak} 100 K | E1-H1 100 K | E1-CB 100 K | H1-VB 100 K | J_T 100 K |
|--------|---------------------------------------|--|------------|-------------|--------------------------|-------------|-------------|-------------|-------------|
| LA | $x = 0.30$ | $p = 0.09, q = 0.16$ | $r = 0.18$ | 0.55 | 375 | 355 | 84 | 55 | 636 |
| LB | $x = 0.30$ | $p = 0.11, q = 0.17$ | $r = 0.19$ | 0.62 | 363 | 339 | 125 | 69 | 226 |
| LC | $x = 0.38$ | $p = 0.15, q = 0.19$ | $r = 0.22$ | 0.78 | 391 | 369 | 186 | 98 | 484 |
| LD | $x = 0.35$ | $p = 0.21, q = 0.12$ | $r = 0.16$ | 1.1 | 393 | 364 | 232 | 137 | 261 |

Fig. 16.3 Measured PL signal, at 12 K, from MQW samples PA, PB, PC and PD. The inset is a plot of the energy at which the maximum PL signal occurs, together with the integrated PL intensity, as a function of QW strain



16.3 Results

Figure 16.3 shows the photoluminescence intensity measured at 12 K for each of the four samples. An Ar^+ ion laser (514 nm) was used to excite the samples with a maximum excitation power density at the sample of 2 W/cm^2 . The maximum in PL intensity was estimated to occur at 364, 373, 383 and 396 meV (corresponding to wavelengths of 3.41, 3.33, 3.24, and 3.13 μm) for samples PA, PB, PC, and PD respectively. The corresponding energies at which the maximum PL intensity was obtained is plotted as a function of the QW strain in the inset of Fig. 16.3 and these energies show a monotonic dependence on the QW strain. An 8 band k,p model was used to calculate the energy levels within the QW, with strain taken into account [11] and material parameters taken from [12] giving values of the E1-H1 transition as 352, 378, 383, and 403 meV for samples PA, PB, PC, and PD respectively, in close agreement to the measured values, as summarised in Table 16.1.

The full width at half maximum (FWHM) of the PL signal at 12 K was estimated to be 14, 31, 18 and 38 meV for samples PA, PB, PC, and PD. These values are of the same order as those obtained, for example, from $\text{GaInAsSb}-\text{AlGaAsSb}$ samples grown on GaSb [13], indicating that growth of high quality $\text{AlGaInSb}/\text{GaInSb}$ quantum wells is possible on lattice miss-matched GaAs substrates, offering potential advantages in terms of cost and integration. However, the surface morphology

of sample PD was not as good as that of the other samples, as the growth was not fully optimised for the highest Al compositions at the time when these samples were grown. This may explain the relatively large FWHM obtained from this sample (the reason for the relatively high FWHM obtained for sample PB is not known).

The PL intensity was measured up to room temperature, and observed to decrease with increasing temperature, for all samples. The integrated PL signal from sample PC is plotted as a function of temperature in Fig. 16.4.

The inset is the Arrhenius plot of the same data. There appears to be a regime with an activation energy of ≈ 40 meV at high temperatures, and a regime at low temperatures where the activation energy asymptotically approaches 0 meV. Similar behaviour is observed in the other samples, and also in other material systems, where the high temperature activation energy is thought to correspond to the thermally activated escape of carriers from the quantum well [14]. However, in our case this activation energy is much smaller than the energy difference between the lowest energy QW electron (E1) subband and the barrier conduction band, and the energy difference between the lowest energy QW hole (H1) subband and the barrier valence band (which is greater than ≈ 100 meV in all samples in each case, as shown in Table 16.1). As the value of activation energy extracted is consistent with the calculated energy separation of the lowest and first excited hole subbands, it is possible higher hole subbands could start to become populated as the temperature increases (we assume that most of the PL signal originates from the E1-H1 transition and that the other electron subbands are not populated under these pumping conditions). Greater population of the higher energy hole subbands could lead to a reduced PL signal in several ways: the reduced population of the lowest hole subband leads to reduced E1-H1 recombination, the optical strength of the transitions between E1 to excited hole subbands is weaker, and finally additional non-radiative Auger processes become available.

In Fig. 16.5, the integrated PL intensity (for sample PD) is plotted as a function of laser excitation power. The integrated PL intensity is plotted on a log-log scale, together with linear fits, showing that the integrated PL intensity I_{PL} is related to the excitation intensity I_{EX} by $I_{PL} \propto I_{EX}^\alpha$, as predicted from analysis of the appropriate rate equations [15]. In this case, the value of α was found to be 1, 1.53, 1.69 and 1.61 at 4, 80, 130 and 180 K respectively, suggesting that at low temperature the luminescence is dominated by exciton recombination [15], and at high temperatures it is dominated by a mixture of free carrier recombination and exciton recombination. Similar behaviour was exhibited by the other samples, with values of α at 4 K/80 K for samples PA, PB, and PC of 1.39/1.89, 1.12/1.69 and 1.19/1.61 respectively. A number of devices, each containing five ridge lasers, were fabricated from each laser structure. Ridges with sloping sidewalls and a width of $\sim 30\text{ }\mu\text{m}$ at the active region were defined using contact photolithography and wet chemical etching. The devices were cleaved to cavity lengths of 2 mm and hand soldered, using indium, substrate-side-down onto coated copper blocks. The facets were neither polished or coated. Figure 16.6 shows the measured spectra from a laser fabricated from structure LD at 100 and 200 K, acquired using a Bentham M300 grating spectrometer, with a resolution of ~ 1 nm, and with the device mounted on the cold finger

of a continuous flow liquid helium cryostat. The device was driven with a 10 kHz square wave with a 1 duty cycle (pulse length = 1 μ s) and with a peak current of 2 A. At 100 K a number of longitudinal modes can be observed. The peak in emittance at 200 K, where wider slit-widths on the spectrometer were used therefore limiting the spectral resolution, occurred at an energy of 376 meV, corresponding to a wavelength of 3.30 μ m. At 100 K the maximum in intensity was estimated to occur at 375, 363, 391 and 393 meV for structures LA, LB, LC, and LD respectively (based on the average from a number of lasers fabricated from each structure), compared to calculated values of the E1-H1 transition of 355, 339, 369 and 364 meV, as summarised in Table 16.2. The predicted spontaneous emission wavelength (E1-H1) for structure LD is plotted as a function of temperature in the inset of Fig. 16.6, indicating that room temperature emission would occur at a wavelength between 3.6 and 3.9 μ m from this structure.

Fig. 16.4 Temperature dependence of the integrated PL signal from sample PC (the line is a guide to the eye only). The same experimental data is shown in an Arrhenius plot in the inset, with a linear least squares fit to the data at high temperatures

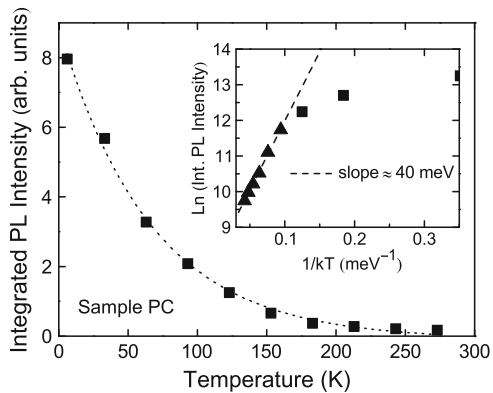
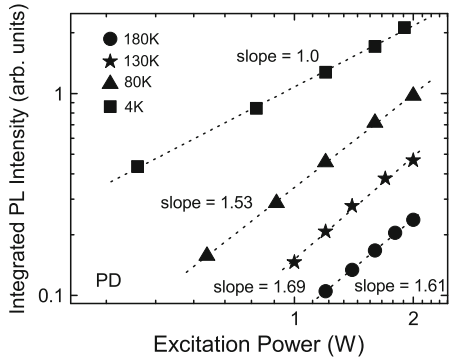
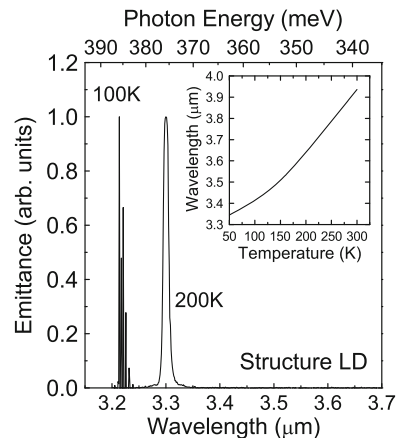


Fig. 16.5 Integrated PL signal from sample PD plotted as a function of incident laser power (P_{EX}), on log scales as a function of temperature. The dotted lines are linear least squares fits to the data



The light-current characteristics of a number of lasers, from different devices, from each structure were measured as a function of temperature, with the device mounted on the cold-finger of a closed cycle cryostat and driven with a 1 kHz square wave with a 1 duty cycle (pulse length \approx 100 ns). In Fig. 16.7 the highest temperature

Fig. 16.6 Measured emission spectra as a function of temperature for a laser fabricated from structure LD. The inset shows the predicted emission wavelength as a function of temperature



at which a clear threshold current was observed (T_{max}) from 45 lasers is plotted as a function of strain in the quantum well. The highest T_{max} obtained from structures LA, LB, LC and LD was 161, 208, 219, and 202 K respectively. The lowest values of T_{max} were obtained from the structure with the lowest value of strain, structure LA, whereas lasers from each of the other structures exhibited a clear threshold current at temperatures above 200 K. Facet polishing experiments suggest that the variation in maximum lasing temperature between different lasers fabricated from the same structure is due primarily to variations in the facet quality, which can be significantly improved by thinning of the wafer before cleaving.

Figure 16.8 shows the plot of the laser emission L versus current density J as a function of temperature for the laser from structure LC with the highest T_{max} . Threshold current densities were extracted from the data shown in Fig. 16.7 by a linear fit to the points above threshold and are shown on a logarithmic scale as a function of temperature in the inset. Threshold current densities were similarly extracted for all devices from the plots of L versus J and the average threshold current densities at 100 K for all the samples are given in Table 16.2. The highest

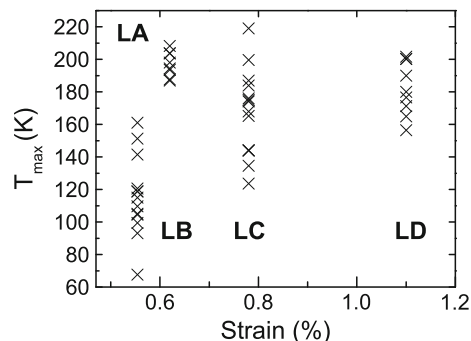
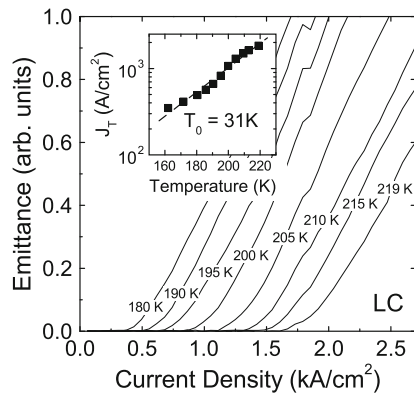


Fig. 16.7 Maximum lasing temperature of different lasers fabricated from the four different laser structures

average threshold current density, 636 A/cm^2 was obtained from structure LA (lowest strain), similar average values were obtained from structures LB and LD (226 and 261 A/cm^2 respectively), and an average value of 484 A/cm^2 was obtained from structure LC. However, the lowest threshold current density at 100 K from any laser, 67 A/cm^2 , was obtained from structure LD. This value is comparable to the value of 40 A/cm^2 obtained previously from 2 mm long GaInSb/AlGaInSb QW diode lasers with a similar composition [16], and emitting at comparable wavelengths at this temperature, but grown on InSb substrates. The value of the characteristic temperature T_0 obtained from the data given in Fig. 16.8, 31 K , is typical of the values obtained from structures LB, LC, and LD over this temperature range, and is also comparable to the value of 38 K obtained from the lasers previously grown on InSb [16].

This value of T_0 is also consistent with previous theoretical studies of similar structures carried out by Andreev *et al* [11], who used an 8 band k.P model to calculate the Auger recombination and optical absorption coefficients in the active region, as well as the gain and threshold characteristics. For quantum wells with similar strain these calculations showed that the relatively strong temperature dependence of the threshold current arises from the strong temperature dependence of the gain (and absorption in the well) which causes the threshold carrier density N_{th} to increase quickly with increasing temperature. As the Auger contribution to the threshold current, J_T^A , is proportional to N_{th}^3 , this also leads to a relatively rapid rise in the threshold current density.

Fig. 16.8 Light-current characteristics as a function of temperature measured for the laser with the highest operating temperature. The inset shows the threshold current densities, J_T , extracted from the data by a linear fit to the points above threshold, as a function of temperature. The line is a least squares fit, yielding a T_0 value of 31 K



Extrapolating the fit of the data shown in the inset of Fig. 16.8 yields an estimated threshold current density of $\sim 10 \text{ kA/cm}^2$ at room temperature. Although this is larger than the value of $\sim 0.5 \text{ kA/cm}^2$ obtained recently from a similar GaSb type-I structure [17] emitting at shorter wavelengths, and which also had 1.6% strain in the quantum wells, Andreev *et al* [11] predicted that the threshold current density will fall significantly, on increasing the strain in the QW active region of GaInSb/AlGaInSb lasers from 1% to 1.5% , due to an increase in the gain (arising from a lifting of the heavy/light hole degeneracy and thereby a better matching

to the electron density of states), a corresponding decrease in N_{th} , and therefore a rapid reduction in Auger recombination (which is proportional to N_{th}^3). The relatively large energy difference between the lowest energy QW hole (H1) subband and the barrier valence band (which is greater than $\simeq 50$ meV in all samples in each case, as shown in Table 16.2) also suggests that hole escape from the quantum well does not limit the temperature at which lasing occurs in these lasers, and Shterengas *et al.* [17] have also recently shown that increasing the number of quantum wells from two to four decreases the threshold current of GaSb type-I lasers above temperatures of 240 K. Coupled with improvements to the device mounting, and facet cleaving and coating, this suggests that there is still significant scope to improve the performance of these lasers further.

16.4 Conclusions

Photoluminescence has been observed up to room temperature from GaInSb Type I multi-quantum well samples, grown onto GaAs. Lasing has been observed up to a temperature of 219 K from diode lasers fabricated from similar structures containing two quantum wells, again grown on GaAs, with the lowest threshold current density obtained from a laser fabricated from the structure with the highest quantum well strain (1.1%). Further improvements to the diode mounting, facet polishing and coating, together with the optimisation of the number of wells and the realisation of quantum wells with higher strain, offer the prospect of significant improvements to the performance of lasers fabricated from the exciting aluminium-gallium-indium-antimonide material system.

Acknowledgements The author would like to acknowledge the work of T. Ashley, L. Buckle, S. D. Coomber, M. T. Emeny, H. Forman, A. Keir, S. J. Smith, C. J. Storey, and G. M. Williams from QinetiQ in Malvern, S. J. B. Przeslak (University of Bristol), P. J. Carrington, A. Krier, and M. Yin (Lancaster University), G. de Valicourt (now at Alcatel-Thales III-V Laboratory), and A. D. Andreev (University of Surrey).

References

- [1] M. Razeghi, M.: High-Performance InP-Based Mid-IR Quantum Cascade Lasers. *IEEE J. Sel. Top. Quantum Electron.* **15**, 941–951 (2009)
- [2] Devenson, J., Teissier, R., Cathabard, O., Baranov, A.N.: InAs/AlSb quantum cascade lasers emitting below $3\mu\text{m}$. *Appl. Phys. Lett.* **90**, 111118 (2007).
- [3] Yang, Q., Manz, C., Bronner, W., Lehmann, N., Fuchs, F., Köhler, K., Wagner, J.: High peak-power (10.5 W) GaInAs/AlGaAsSb quantum-cascade lasers emitting at $\lambda \simeq 3.6$ to $3.8\mu\text{m}$. *Appl. Phys. Lett.* **90**, 121134 (2007).
- [4] Zhang, S.Y., Revin, D.G., Commin, J.P., Kennedy, K., Krysa, A.B., Cockburn, J.W.: Room temperature $\lambda \simeq 3.3\mu\text{m}$ InP-based InGaAs/AlAs(Sb) quantum cascade lasers. *Electron. Lett.* **46**, 439-440 (2010).

- [5] Vurgaftman, I., Canedy, C.L., Kim, C.S., Kim, M., Bewley, W.W., Lindle, J. R., Abell, J., Meyer, J.R.: Mid-infrared interband cascade lasers operating at ambient temperatures. *New. J. Phys.* **11**, 125015 (2009).
- [6] Hosoda, T., Kipshidze, G., Tsvid, G., Shterengas, L., Belenky, G.: Type-I GaSb-Based Laser Diodes Operating in 3.1 to $3.3\mu\text{m}$ Wavelength Range. *IEEE Photon. Technol. Lett.* **22**, 718-720 (2010).
- [7] Nash, G.R., Smith, S.J., Coomber, S.D., Przeslak, S., Andreev, A., Carrington, P., Yin, M., Krier, A., Buckle, L., Emeny, M.T., Ashley, T.: Midinfrared GaInSb/AlGaInSb quantum well laser diodes grown on GaAs. *Appl. Phys. Lett.* **91**, 131118 (2007).
- [8] Shterengas, L., Belenky, G., Kisim, M. V., Donetsky, D.: High power $2.4\mu\text{m}$ heavily strained type-I quantum well GaSb-based diode lasers with more than 1W of continuous wave output power and a maximum power-conversion efficiency of 17.5%. *Appl. Phys. Lett.* **90**, 011119 (2007).
- [9] Yin, M., Nash, G.R., Coomber, S.D., Buckle, L., Carrington, P.J., Krier, A., Andreev, A., Przeslak, S.J.B., de Valicourt, G., Smith, S.J., Emeny, M.T., Ashley, T.: GaInSb/AlInSb multi-quantum-wells for mid-infrared lasers. *Appl. Phys. Lett.* **93**, 121106 (2008).
- [10] Nash, G.R., Przeslak, S.J.B., Smith, S.J., de Valicourt, G., Andreev, A.D., Carrington, P.J., Yin, M., Krier, A., Coomber, S.D., Buckle, L., Emeny, M.T., Ashley, T.: Midinfrared GaInSb/AlGaInSb quantum well laser diodes operating above 200K. *Appl. Phys. Lett.* **94**, 091111 (2009).
- [11] Andreev, A.D., O'Reilly, E.P., Adams, A.R., Ashley, T.: Theoretical performance and structure optimization of 3.5 to $4.5\mu\text{m}$ InGaSb/InGaAlSb multiple-quantum-well lasers. *Appl. Phys. Lett.* **78**, 2640-2642 (2001).
- [12] Vurgaftman, I., Meyer, J.R., Ram-Mohan, L.R.: Band parameters for III-V compound semiconductors and their alloys. *J. Appl. Phys.* **89**, 5815-5875 (2001).
- [13] Rainò, G., Salhi, A., Tasco, V., Intartaglia, R., Cingolani, R., Rouillard, Y., Tournié, E., De Giorgi, M.: Subpicosecond timescale carrier dynamics in GaInAsSb/AlGaAsSb double quantum wells emitting at $2.3\mu\text{m}$. *Appl. Phys. Lett.* **92**, 101931 (2008).
- [14] Pannekamp, J., Weber, S., Limmer, W., Sauer, R.: Temperature and excitation-density-dependent photoluminescence in a GaAs/AlGaAs quantum well. *J. Luminescence* **85**, 37-43 (1999).
- [15] Fouquet, J.E., Siegman, A.E.: Room-temperature photoluminescence times in a GaAs/ $\text{Al}_x\text{Ga}_{1-x}\text{As}$ molecular beam epitaxy multiple quantum well structure. *Appl. Phys. Lett.* **46**, 280-282 (1985).
- [16] Ashley, T.: Type-I InSb-based mid-infrared diode lasers. *Phil. Trans. R. Soc. Lond. A* **359**, 475-488 (2001).
- [17] Shterengas, L., Belenky, G., Hosoda, T., Kipshidze, G., Suchalkin, S.: Continuous wave operation of diode lasers at $3.36\mu\text{m}$ at 12°C . *Appl. Phys. Lett.* **93**, 011103 (2008).